UCLA
UCLA Electronic Theses and Dissertations

Title
Radiofrequency Encoded Angular-Resolved Light Scattering

Permalink
https://escholarship.org/uc/item/50x3v096

Author
Akbari, Najva

Publication Date
2015

Peer reviewed|Thesis/dissertation

eScholarship.org Powered by the California Digital Library
University of California

UNIVERSITY OF CALIFORNIA
Los Angeles

Radiofrequency Encoded Angular-Resolved Light Scattering

A thesis submitted in partial satisfaction
of the requirements for the degree
Master of Science in Electrical Engineering
by

Najva Akbari

2015

© Copyright by

Najva Akbari

2015

ABSTRACT OF THE THESIS

Radiofrequency Encoded Angular-Resolved Light Scattering

by

Najva Akbari

Master of Science in Electrical Engineering

University of California, Los Angeles, 2015

Professor Bahram Jalali, Chair

Label-free classification of microstructures is a valuable approach in a variety of fields including cytometry and atmospheric science. The sensitive classification of microscopic cells and organisms is especially an important outstanding problem in biology. Flow cytometry is a routine method for cell classification. Current flow cytometers use light scattering at two fixed angles to infer information about size and internal complexity of cells at rates of more than 10,000 cells per second. However, this approach limits the precision and information that can be deduced by the cell population from the light scattering patterns. Capturing the full angular scattering spectrum of cells and particles would enable classification of cells with higher resolution and specificity. By capturing the angular dependence of scattering intensity we will be able to extract information about the scattering particle, hence providing a label-free method for particle classification. Current

systems that provide angular scattering patterns do not have the throughput required to be implemented in state-of-the-art flow cytometers.

Inverse scattering has been one of the more difficult problems to solve in electromagnetic wave interaction problems. Yet there have been many solutions obtained by analytical and computational modeling for various cases. The angular light scattering profile of particles is dependent on their morphological parameters, such as size, shape, and their internal structure. One of the most interesting applications of modeling these scattering profiles is in characterizing cells to identify abnormalities. Methods to take advantage of this angular dependent information have been demonstrated, however, these methods have various limitations such as low speed and precision. Here I present a new high throughput multi-angle resolved light scattering measurement technique that is able to capture the full angular scattering profile of particles in a single shot using a single detector. Termed Radiofrequency Encoded Angular-resolved Light Scattering (REALS), this technique uses one-to-one radiofrequency-to-angle mapping to measure angular dependence of light scattered from particles in a single shot using a photomultiplier tube. Using this technique it is possible to capture the continuous scattering profile over a wide dynamic range without mechanical scanning. This information allows us to characterize particle morphology and size with increased accuracy and high throughput, enabling label-free and high speed flow cytometry. As a proof of concept we distinguish the radius of tapered silica fiber over a range of radii.

The thesis of Najva Akbari is approved.

Bahram Jalali

Warren S. Grundfest

Aydogan Ozcan

University of California, Los Angeles

2015

DEDICATION

To my mother for her never-ending love and strength.

Contents

Table of Figures

Literature Review

Flow Cytometry – Applications + Short Comings

Flow cytometry is a widely used method in probing biological systems using fluorescence or scattering patterns. Flow cytometers perform multi-parameter measurements on each cell, allowing for precise sorting. Multiple fluorescent agents are used as markers for parameters of interest which require long processing time. Scattering measurements are another group of parameters widely used in state of the art flow cytometers for non-invasive and label-free particle classification. These systems, however, typically measure at only two angles: forward and side scatter. The scattered light from cells is generally focused onto two detectors at fixed angles by two collecting lenses. These systems integrate the scattered intensity over a range of angles (depending on the acceptance angle of the collecting lenses) onto the detectors. Such systems fail to recover much of the detailed information encoded in the full scattering profile. An example of scattering-based classification can be seen in the figure below:

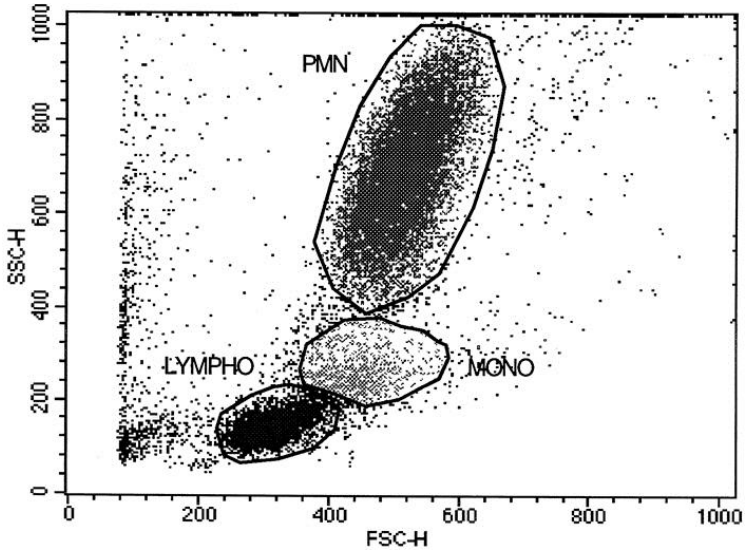

Figure 1 Example of cytogram. Hydrogen Peroxide Production in Leukocytes during Cerebral Hypoxia and Reoxygenation with 100% or 21% Oxygen in Newborn Piglets.[1]

The angular light scattering profile of cells and microscopic particles encodes significant information of their biochemical structure and morphological properties, such as size, shape and internal complexity.[2] Intensity of small scattering angles ($\theta < 2°$) strongly depends on cell size and refractive index.[3] These cell parameters have been used as indicators for cell abnormalities as well as for cell counting. At larger angles ($5° < \theta < 30°$) the intensity of scattered light depends on nucleus to whole cell volume ratio. Such information is used for a variety of applications including cancerous cell detection.[4] Further information can be deduced about the internal structure of cells at higher angles ($50° < \theta < 130°$). The cell organelles act as additional scattering sites within the cells and hence add more to the scattering at higher angles. This information may be valuable for drug development purposes where different agents vary the internal structure of cells.[5] The backscattering region ($160° < \theta < 180°$) also provides valuable information about the cell membrane which is an indicator for cell viability.[6]

Increasing the resolution of the angular measurement so as to resolve the full scattering profile could enable more accurate and sensitive particle classification. Systems with capability to record angular scattering patterns have been developed but suffer from fundamental limitations such as low speed of mechanical scanning and low count of photons at large scattering angles. These instruments resolve the full angular scattering profile, via scanning flow cytometry (SFC), such as the mechanical scanning or goniometric approach[7], flying light scattering indicatrix method (FLSI)[8,9], and the liquid-core-waveguide based method.[10] The throughput limitations of such systems obstructs their integration with current state-of-the-art flow cytometers and hence call for a better system to collect this information.

A recently developed technique, termed Spectrally Encoded Angular-resolved Light Scattering (SEALS)[11], addresses this full-spectrum scattering measurement problem in a high

throughput fashion using an ultrafast optical approach. Inspired by a high-throughput bright field imaging technique, Serial Time Encoded Amplified Microscopy (STEAM)[12], SEALS uses a one-to-one scatter angle-to-optical wavelength mapping to encode the angular scattering profile onto the spectrum of a broadband ultrafast optical pulse. Using the dispersive Fourier transform (DFT)[13] and a single high speed photodetector, the entire angular scattering spectrum can be read on a single shot basis in real time at MHz repetition rates. Additionally, using a digitally programmable optical filter, SEALS pre-equalizes the intensity of the optical spectrum to compensate for the discrepancy in scattering intensities between forward and side scattered light, improving the system dynamic range. With the MHz frame rates and large dynamic range of SEALS, however, come increased component and system complexity. The reliance on a modelocked laser and dispersive optics in particular limit the usefulness of SEALS to only the most bandwidth intensive applications. Implementation of this system is shown in Figure 2.

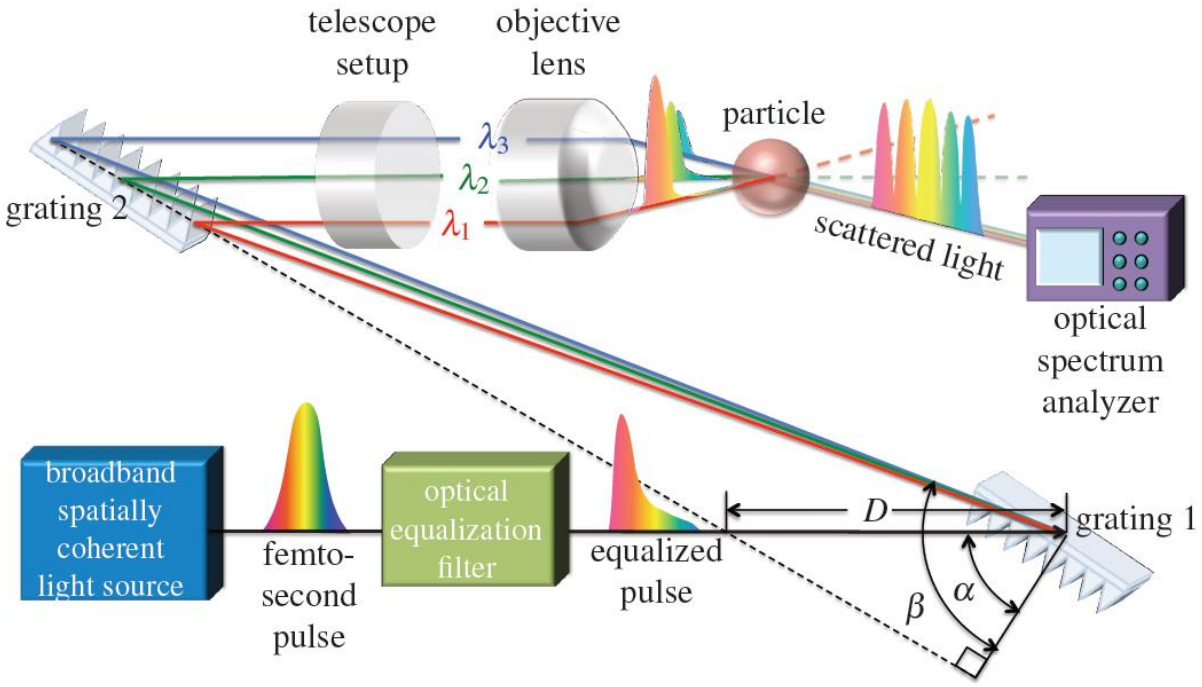

Figure 2 Schematics for the STEAM system. An optical pulse is created by a broadband pulsed laser. The power spectrum of the illuminating light is modified with an optical filter to provide more power to optical frequencies corresponding to side scattering angles. Next, the broadband optical pulse is converted into a collimated one-dimensional rainbow using a pair of diffraction gratings. A telescope setup is used to adjust the beam size. The resulting one-dimensional rainbow is focused onto particles under test, by a high-NA objective lens (60x, NA=0.7). The particle is hence illuminated by light at different angles and scattered light is measured at a single, fixed angle. The output is then directly fed into an optical spectrum analyzer (OSA) via a multimode fiber.

In this paper I will introduce a new method, inspired by SEALS, which can capture the full angular scattering patterns of particles in a single shot by mapping the angular information to RF frequencies.

Inverse Scattering Problem

Because many cells and particles are comparable in size to wavelengths that are used in imaging and flow cytometry, electromagnetic (EM) methods are required to describe the scattering in these systems. EM interaction problems can be divided into two groups of direct or forward problems and inverse problems. In general there are two sides to an EM interaction problem: the governing equations and the physical data. In the case of direct scattering problems, the fields are determined

by knowing the governing equations as well as the media information (i.e. the boundary and initial conditions, geometry, etc). In inverse scattering problems however, partial information about the field is known and the goal is to determine the media from which the field is generated from. The inverse scattering problem is the more frequently faced and unfortunately the more challenging problem. The information available is generally limited. For example, the field inside the particle, which is necessary to specify a particle uniquely, is usually not accessible.

In order to solve these problems, supplementary information is used in addition to the available scattered field information. Polarization properties and known geometries of particles are a few of such pre-known information. In many experiments, for example, the inverse problem is solved by minimizing the weighted sum of squares:

$$S(\beta) = \sum_{i=1}^{N} z_i^2 \ , \qquad z_i = w(\theta_i)\left[I_{th}(\theta_i, \beta) - I_{\exp} \quad (\theta_i)\right]$$

In this presentation of the problem, β is a vector of p model parameters, and I_{th} and $I_{\exp}$ are the theoretical and experimental light scattering profiles. This approach has been applied to classification of both spherical and non-spherical particles in applications such as E. Coli and milk fat globule characterization.[14,15] The theoretical values for this solution are found through Mie theory. In fact, Mie theory is one of the most important and well known solutions to an exactly solvable problem in scattering for small spherical particles with arbitrary radii and refractive index. This solution is the basis for many applications in a variety of fields including astrophysics and biophysics. Generally a library of scattering profiles is created through numerical analysis methods (e.g. FDTD) and the experimental data is compared to the library for classification.

Another exact solution to the problem of scattering and absorption can be found for infinitely long right circular cylinder. Many naturally occurring particles have the form of a cylinder and hence this solution is also of valuable use in scattering problems. The simplest form of this solution is found for an incident electric field parallel to the axis of the cylinder when the incident light is normal to the cylinder axis. In this case the electric field expansion can be found from the following equations[16]:

Scalar wave equation in cylindrical coordinates

$$\frac{1}{r}\frac{\partial}{\partial r}\left(r\frac{\partial \psi}{\partial r}\right)+\frac{1}{r^2}\frac{\partial^2 \psi}{\partial \Phi^2}+\frac{\partial^2 \psi}{\partial z^2}+k^2\psi=0$$

Vector cylindrical harmonics

$$M_n = \nabla \times (\,\hat{e_z}\ \psi_n\,),\ \ N_n = \frac{\nabla \times M_n}{k}$$

Resulting scattered field expansion

$$E_s = -\sum_{n=-\infty}^{\infty} E_n b_{nI} N_n^{(3)}$$

$$b_{nI}(\xi = 90°) = b_n = \frac{J_n(mx)J_n'(x) - mJ_n'(mx)\,J_n(x)}{J_n(mx)H_n^{(1)'}(x) - mJ_n'(mx)H_n^{(1)}(x)}\ ,\quad x = ka$$

Where $J_n(\rho)$ is the Bessel function, $H_n^{(1)}$ is the Hankel function, and m is the refractive index of the cylinder relative to the surrounding medium. Based on the scattered field we can find a phase function to be the fraction of the scattered light that is scattered into a unit solid angle about a given direction (θ, Φ). In order to demonstrate the angular dependence of the phase and hence the angular scattering let's consider a cylinder that is large enough to be in the diffraction theory

approximation limit. We can derive the phase function for the incident beam in the above scenario to be:

$$p = \sin^2(xsin\theta)\, p_e(\theta, 90°) = sin^2(xsin\theta)\frac{\left(\frac{1+cos\theta}{2}\right)^2 p(0°)}{x^2 \sin^2\theta}$$

The phase function is the fraction of the total scattered light that is scattered into a unit solid angle about a given direction (θ, Φ). We can observe a periodic angular dependence as shown in figure below:[16]

The periodicity of the scattered field is an indicator of particle size when other factors have not been changed. In our proof of concept demonstration of REALS, we have used this indicator to distinguish between varying diameters of a tapered Silica fiber.

Frequency Domain Multiplexing

The field of imaging and communication have long shared a similar mathematic tool set. Namely the technique of frequency analysis has allowed significant advancements in both fields and provided a basis for quantification. The fundamental reason for this similarity has been the linearity and invariance properties. These properties allow for considerable simplification in studying complex systems by decomposing inputs into elementary stimuli and predicting the outcome based on response to elementary inputs. This mathematical approach also plays a key role in synthesizing signals for various applications and in various fields. One of the most well-known applications, for examples, is for achieving high data rates in modern optical communication through wavelength-division multiplexing (WDM)[17]. WDM in fibers allows for simultaneous transmission of many orthogonal channels onto a single common medium. In WDM optical signals with slightly different wavelengths are combined and transmitted from the transmitter end and received and

decomposed in the receiver side. In this method each channel is mapped to a different frequency, allowing for orthogonal multiplexing which improves the speed of the system in several-fold. The mentioned approach of orthogonal information mapping is not restricted to modern optical communication but is used in a variety of fields. In our system we have used this approach to map scattering angle of beams to orthogonal RF frequencies. This approach allows us to multiplex the angular scattering spectrum of objects into a time domain signal that can be captured by a photomultiplier tube. The signal can then be decomposed into constituent elements using Fast Fourier Transform (FFT). The frequency distribution within each frame gives us the intensity information corresponding to angular scattering of objects. By incorporating this approach we are able to increase the speed of information acquisition, thus creating a system that is compatible with current needs in flow cytometry. To implement the mentioned multiplexing, we take advantage of the phenomena of acousto-optic interaction as well as interference.

Acousto-Optic Effect

The acousto-optic effect is a nonlinear optical effect by which the optical frequency is varied through scattering by acoustic waves. This effect is created by causing a periodic change in the refractive index of the medium through which light travels. This periodic change is cause by the presence of a sound wave in the medium. The acoustic frequencies fall into two categories of hypersonic and ultrasonic waves. While hypersonic waves are caused by thermal excitation, ultrasonic waves are excited electronically through piezoelectric transducers. The ultrasonic frequency region falls between 100 kHz and a few gigahertz. A very interesting and useful property of using acoustic waves to create refractive index gratings is the ability to control the frequency and modulation depth by controlling the frequency and amplitude of the electronic signal that is being applied to the piezoelectric transducer. This electronically controllable property makes it

very convenient to use this phenomena for a variety of applications. Many crystals of interest in acousto-optic applications (e.g. LiNbO3, TeO2) are piezoelectric. The elasto-optic coefficients of such material is modified by the piezoelectric effect. Since the strain produced by an acoustic wave generates an electric field, index variations are also caused by the electro-optic effect. These secondary index variations depend on the direction of propagation of the acoustic wave and can be significant.

The optical properties of media can change due to mechanical strain. This phenomena is referred to as the photoelastic effect. In dynamic photoelastic effect, the optical properties of media are periodically varied in time by an acoustic wave which cause periodic and time dependent mechanical strain. This effect is the basis for acousto-optic interaction. The photoelastic effect can be defined in terms of changes in the relative impermeability tensor caused by strain as follows[18]:

$$\eta_{ij}(\boldsymbol{S}) = \eta_{ij} + \Delta\eta_{ij}(\boldsymbol{S}) = \eta_{ij} + \sum_{k,l} p_{ijkl} S_{kl}$$

The periodic permittivity changes caused by a traveling plane acoustic wave can generally be expressed as

$$\Delta\epsilon = \Delta\tilde{\epsilon}\sin(\boldsymbol{K}.\boldsymbol{r} - \Omega t)$$

In this equation, **S** is the strain tensor and p_{ijkl} are the elasto-optic coefficients. Where $K = \frac{2\pi}{\Lambda}$ and $\Omega = 2\pi f$. Here **K** depends on the polarization and direction of propagation of the acoustic wave. $\Delta\tilde{\epsilon}$ is dependent on the strain caused by the acoustic wave, properties of the acoustic wave, and properties of the optical wave, but is independent of **K** and Ω. When an optical beam with frequency ω interacts with the mentioned environment, diffracted optical beams are generated at frequencies $\omega \pm \Omega$. These diffracted beams can in turn interact with the environment to create

beams at optical frequencies of $\omega \pm 2\Omega$. This process can continue to create optical frequencies of $\omega \pm q\Omega$ where q is the order of the acousto-optic diffraction. With the appropriate setup and design, the first order diffracted beam has the highest efficiency. The angular position of the diffracted beam is linearly proportional to the acoustic frequency and is found by the following equation:

$$\theta = \lambda . \frac{f}{V_a}$$

Here θ is the angle between the incident laser beam and the diffracted laser beam, λ is the optical wavelength in air, and V_a is the acoustic velocity. The value of θ is determined by the phase matching conditions that ensure the conservation of momentum. These concepts are illustrated in the figure below:

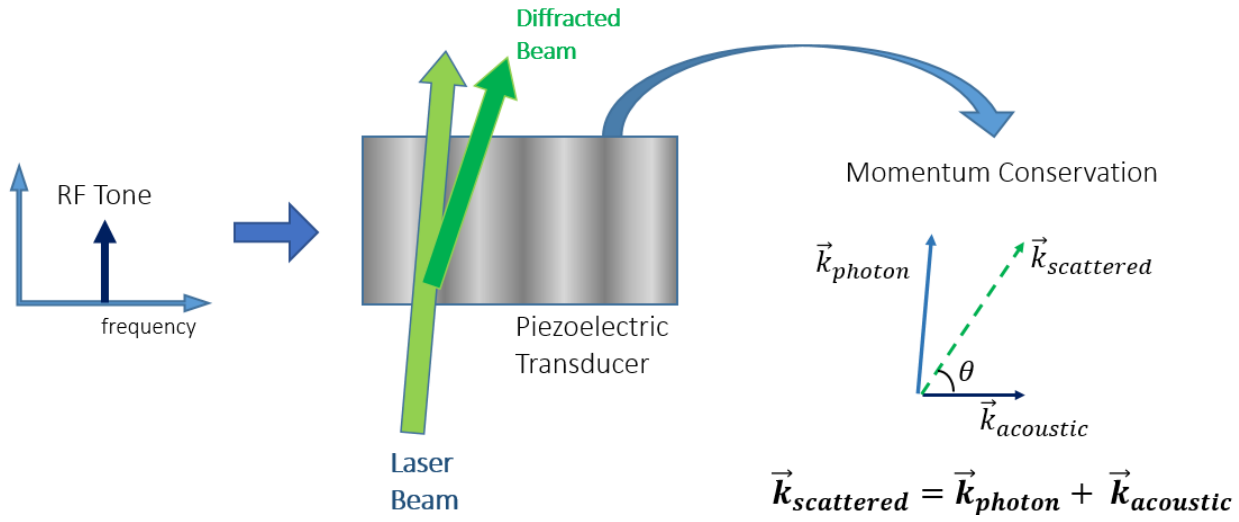

Figure 3 Illustration of acousto-optic interaction. Interaction of light with a piezoelectric transducer.

The intensity of the diffracted beam depends on the power of the RF tone, the material properties, geometrical factors, and wavelength and is expressed by the equation below:

$$\eta = \sin^2\left[\frac{\pi}{\lambda}\left(\frac{M_2 . P_{ac} . L}{2H}\right)^{\frac{1}{2}}\right]$$

Where P_{ac} is the acoustic power, M_2 is the material figure of merit, and L/H is a geometrical factor.

Methodology

System Concept

The central defining idea behind REALS is the mapping of angular information to radiofrequency domain. This method has been inspired by a novel high-speed imaging method: Fluorescence Imaging using Radiofrequency-tagged Emission (FIRE)[19]. Similar to FIRE's approach in mapping the spatial information of an image to radiofrequency domain to increase imaging speed, REALS maps the angular scattering patterns of particles to frequency domain, enabling multiplexing of the signal which greatly increases the speed of acquiring information. The multiplexed signal can be recorded as a time domain signal by a photomultiplier tube (PMT) and the signal can be analyzed to obtain the scattering profile using an electrical spectrum analyzer. Alternatively, the signal can be digitized in real time and analyzed using digital frequency domain techniques such as fast Fourier transform (FFT). This method also enables achieving a high dynamic range in the full angular distribution by allowing for digital pre-equalization of RF frequency intensities and hence overcoming the power roll off at higher scattering angles. In addition, REALS is implemented using conventional optics and acousto-optic devices, making it a simple and robust design for practical purposes.

Light is incident on the sample from a range of discrete, radiofrequency-tagged angles and a single element detector collects the scattered light from a single position. The scattered beams interfere

with the LO beam at the PMT and as a result the frequency components of the collected signal give us the angular scattering spectrum of the sample. By illuminating the sample with multiple transverse optical k-vectors (k_{RF}) and detecting the light scattered into a single direction (k_{PMT}), the spatial frequency (k_{sample}) of the sample is recovered.

Schematic of the REALS implementation can be viewed in figure 4. In this implementation, a continuous wave (CW) laser beam is split into two arms of a Mach-Zehnder interferometer using a polarizing beam splitter, allowing for the control of power in each arm. Each arm contains an acousto-optic device to control the assignments of RF frequencies to the beams. An electronic waveform generator is used together with an amplifier for each of the devices to create the appropriate signal for the transducers. A set of cylindrical lenses are used to focus the beam to fall within the height of the acousto-optic crystal. The frequency shifted beams are focused onto the back aperture of an objective lens so that each point on the back aperture corresponds to an incident angle on the sample. The last mirror of the LO can be translated to adjust the angular location of the LO beam(s). A rotating stage is aligned with the objective lens such that the center of the stage is at the focal point of the objective lens. The sample is placed at the center of the rotating stage and a CMOS camera is used to verify that it is in the focal plane of the objective lens. The photodetector is then placed on the rotating stage such that it can rotate at a fixed radius. The collected beam is narrowed through 2 100-μm pinholes in order to increase angular sensitivity of the system. The signal from the photodetector is amplified using a low noise amplifier and is sent to either an electrical signal analyzer or a digitizer. A delay stage is used to match the optical path length of the two interfering arms.

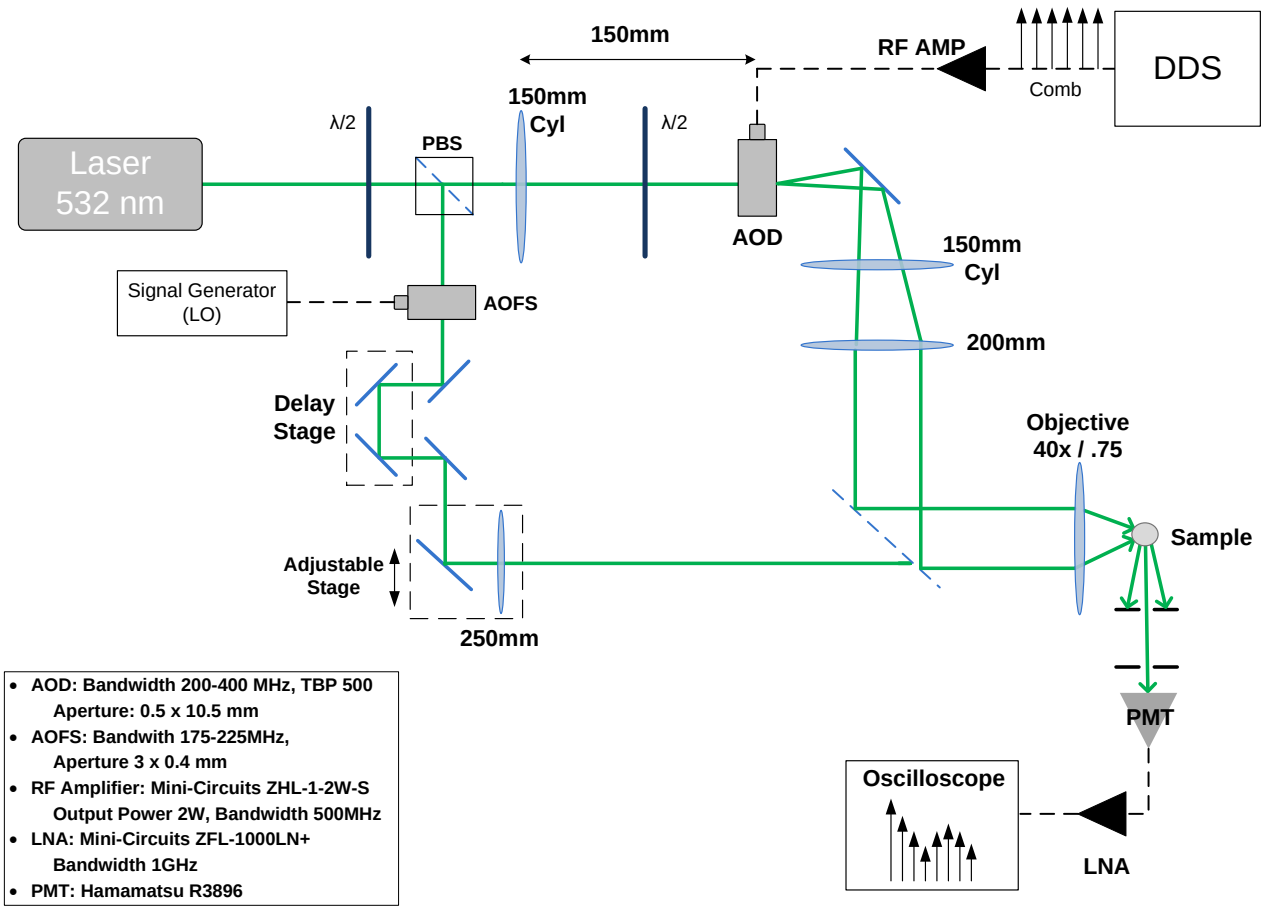

Figure 4 Schematic of the REALS system. A 532-nm CW laser is split into two arms of a Mach-Zehnder interferometer containing two AO devices. The acousto-optic deflector creates multiple frequency-shifted beams in the RF comb arm, which are diffracted at unique angles. These beams are directed to the sample via a tube and objective lens, illuminating the sample from a range of angles. The AOFS generates an LO beam which scatters off of the sample and beats with the scattered RF beams at the detector. The beat signals are detected by a PMT and recorded by a digitizing oscilloscope.

Acousto-Optic Deflectors

There are two acousto-optic devices used in the two arms of the Mach-Zehnder interferometer. The wide bandwidth Acousto-optic deflector (AOD) is used to provide an array of beams frequency shifted by a range of orthogonal RF frequencies. The RF frequencies are generated by direct digital synthesis of a time domain electronic signal which is applied to the piezoelectric transducer.[19] Each RF frequency deflects the beams at a different angle, allowing for separation of the beams. This concept is shown in figure 5. Through the acousto-optic interaction, the laser beam is both deflected at a unique angle per frequency as well as being shifted in optical frequency by

the corresponding RF frequency. The frequency comb signal is phase-engineered through Golay complementary sequence in order to minimize its peak to average ratio.[20] This assures that the power of the RF frequencies does not saturate due to the power limits of the AOD.

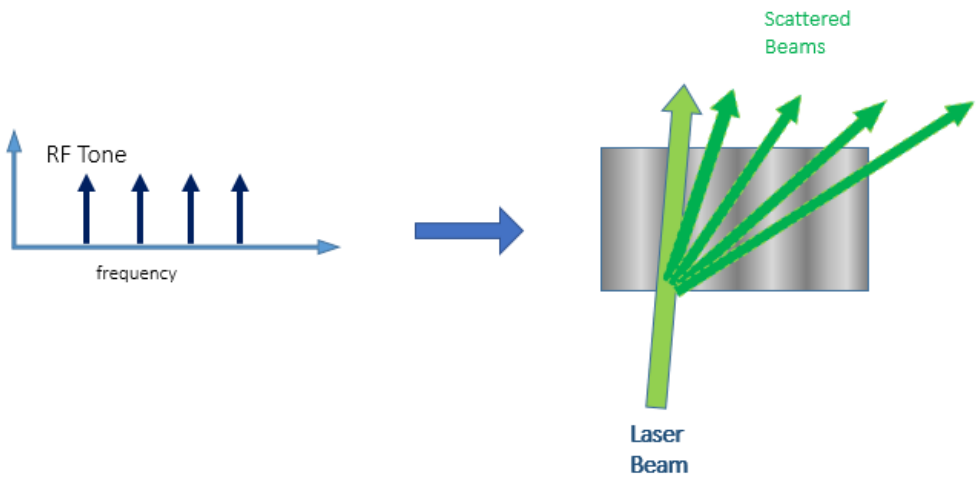

Figure 5 Illustration of acousto-optic interaction. Multiple beams deflect through interaction with a piezoelectric transducer being driven by a signal containing multiple RF frequencies.

In the current setup, as can be viewed in figure 4, the second acousto-optic device is an acousto-optic frequency shifter (AOFS). The beam passing through this device serves as a local oscillator for the heterodyne detection system. The purpose of having an AOFS is to be able to control the range of frequencies detected by the PMT. This convenient design allows for adjusting the frequencies at which the data is captured in order to avoid any noisy frequency range as well as making it possible to comply with the frequency ranges of the other devices in the system.

In the initial design of the system, an AOD was used instead of an AOFS. In this setting the array of beams were aligned to interfere with a corresponding array of beams from the second AOD. In this setting, the beams interfered on the sample and we expected to pick up only the beams that scattered from the interference at the sample. However, we observed that the scattered light also interfered with the other beams at the PMT, causing multiple signal interferences.

To overcome this issue, the design of the setup was changed such that the LO arm of the interferometer contained only an AOFS. By this means a single frequency shifted beam was created to interfere with all of the scattered beams on the PMT so that the signals received from individual scattering angles do not interfere and we are able to correctly retrieve the scattering spectrum.

Photodetection

The photodetector used in the system is a photomultiplier tube (PMT). PMT's have been valuable for a variety of applications. They are extremely sensitive photodetectors, capable of detecting single photons with gains as high as 10^8 times the generated current by a single photon. In addition, unlike many other photodetecting devices, PMT's have very high response rates which make them ideal for high throughput systems. One of the main issues in using PMT's for wide field of view imaging is that they are typically produced in single element formats. With REALS, it is possible to capture parallel information by using the bandwidth of the PMT despite the single element limitations. This approach enables the utilization of the gain and frequency response of the detector, while being simple and practical.

Digital Signal Processing

Since the frequency components of our signal of interest are known, we can implement digital lock-in amplification to retrieve the signal. Lock-in amplification is a technique that allows for detections of small signals. This method enables the detection of signals much smaller than noise level. In this method the AC signal of interest is multiplied by a known reference signal. The combined signal is then low-pass filtered to obtain the DC component that includes amplitude and phase information of the signal.

$$V_{sig}(t) = V_s \sin(\omega t + \varphi_s)$$

$$V_{ref}(t) = V_r \sin(\omega t + \varphi_r)$$

$$V_{mix} = V_{sig}.V_{ref} = \frac{1}{2}V_sV_r \cos(\varphi_r - \varphi_s) + \frac{1}{2}V_sV_r \sin(2\omega t + \varphi_r + \varphi_s)$$

$$V_{mix+fil} = \frac{1}{2}V_sV_r\cos(\varphi_r - \varphi_s)$$

In order to find the signal amplitude without knowing the phase, we can multiply the signal by another reference signal, shifted by $\frac{\pi}{2}$ as follows:

$$V_{ref2}(t) = V_{r2} \sin\left(\omega t + \varphi_r - \frac{\pi}{2}\right)$$

$$V_{mix2} = \frac{1}{2}V_sV_{r2} \cos\left(\varphi_r - \varphi_s - \frac{\pi}{2}\right) + \frac{1}{2}V_sV_{r2} \sin\left(2\omega t + \varphi_r + \varphi_s - \frac{\pi}{2}\right)$$

$$V_{mix2+fil} = \frac{1}{2}V_sV_{r2} \cos\left(\varphi_r - \varphi_s - \frac{\pi}{2}\right) = \frac{1}{2}V_sV_{r2}\sin(\varphi_r - \varphi_s)$$

If $V_{ref} = V_{ref2} \rightarrow$ $\qquad V_{mix+fil}^2 + V_{mix2+fil}^2 = \frac{1}{4}V_s^2V_r^2$

The use of frequency to carry information in REALS allows for use of lock-in amplification for signal reconstruction in the digital domain.

Results

In order to validate and quantify our system performance, we verified the linear RF-to-angle mapping, measured the angular resolution and angular range. The longitudinal TeO_2 AOD was driven with a frequency comb within the range of 305 MHz to 395 MHz with 1MHz spacing. The beam diameter was measured to be 2.2mm at the entrance of the AOD, allowing for use of ~48

TBP from the AOD. To make angular measurements, two 100-μm pinholes and a PMT were placed at a eucentric position on a rotating stage and measurements were made at various angles. The beam array from the AOD was collimated and collected at the back aperture of a 40x, 0.66-NA objective lens. The mentioned frequency comb covered a range of 30º, creating a linear mapping of 0.34º/MHz as can be viewed in figure 6.

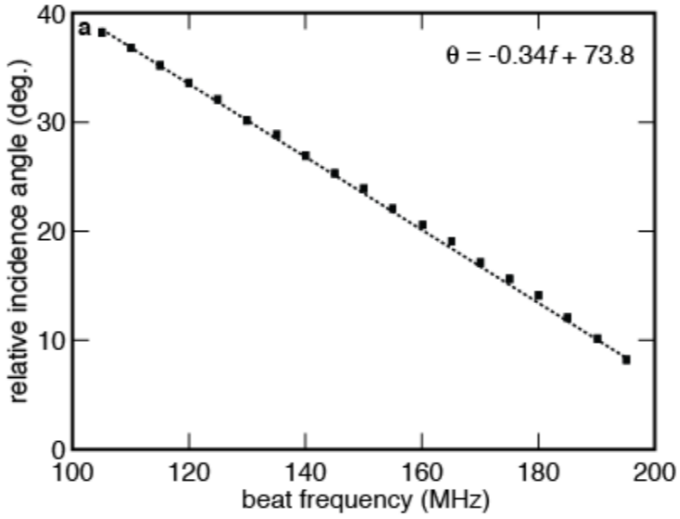

Figure 6 REALS RF-to-angle mapping. Rotating the angular position of the PMT detector module about the focus point provides a measurement of the RF-to-angle mapping of REALS.

The measured angular resolution of the setup is 1.1º (3.48 MHz) which corresponds to approximately 26 resolvable points. This value most likely differs from the theoretical TBP value of 48 due to the additional divergence of the collimated beams after the objective lens as well as the finite aperture size of the pinholes. The angular resolution is demonstrated in figure 7.

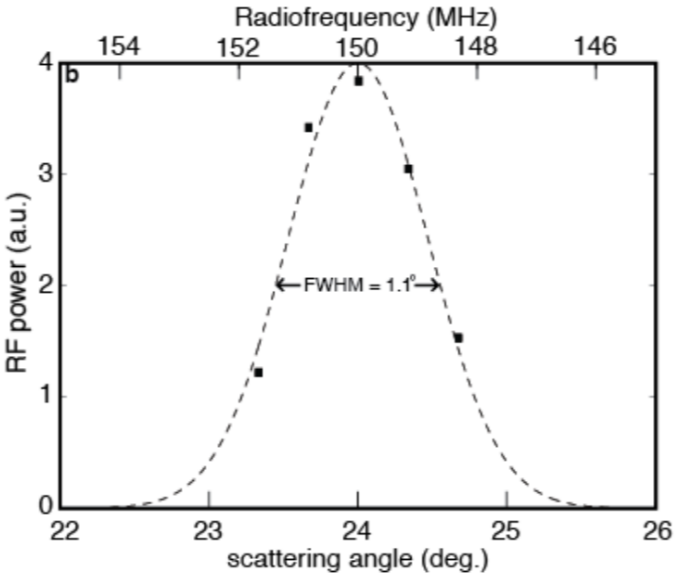

Figure 7 REALS angular resolution. Using the mapping as calibration, the angular resolution of the system can be determined using a Gaussian fit to the data at a single angle.

To account for the drop in power of the higher angles and increase in the dynamic range of the system, the frequency range was chosen such that the intrinsic variance in the efficiency of the AOD would counteract the loss at higher scattering angles. The power variation of the beam without any scattering can be seen in figure 8.

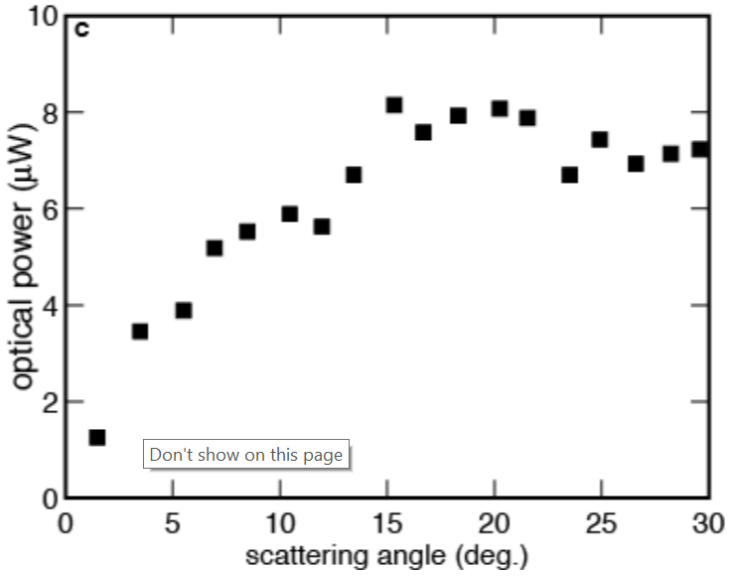

Figure 8 Optical power versus scattering angle. The non-uniform efficiency of the AOD is exploited here to maximize optical power at high scattering angles, and reduce the power at low scattering angles in order to provide pre-equalization and dynamic range improvement.

Measured samples

To demonstrate the performance of REALS in distinguishing sizes of scattering objects, we measured the scattering spectra of a tapered fiber along the direction of the fiber. Because of the cylindrical symmetry, a fiber was chosen for the proof of principle demonstration. As mentioned in the inverse scattering section, because of the symmetry, we have an analytical solution for the angular scattering of cylindrical objects which can be used, with good approximation, to determine the diameter of the scattering object (tapered fiber) used in this setup. This choice of sample object is also appropriate for the potential application of REALS in interrogating particles in flow (i.e. in flow cytometry). The cylindrical shape of the microfluidic channels used in flow cytometry systems is ideal in avoiding refraction from minimizing the angular range of the incident RF-shifted beams as well as from distorting the scattering spectrum.

Our cylindrical sample was created by heating a single mode optical fiber (SMF-28) to its softening point in a hydrogen flame and pulled at a uniform velocity using two linear translational stages.[21] The fiber diameter varied from 5μm to 20μm within the measured data. The tapered fiber was attached to a rigid mount and placed at the focal plane of the objective lens, The PMT detector was placed in line with the LO beam at the forward scatter angle (0º).

The scattering spectra were collected from each position within the range of interest in the tapered fiber using a digital oscilloscope. The spectra were recorded at a rate of 250 kHz, using a frequency comb spacing of 1 MHz. Figures 9 shows the mean and standard deviation of 200 scatter measurements fitted to simulated Mie scattering profiles along with the corresponding fiber image.[16]

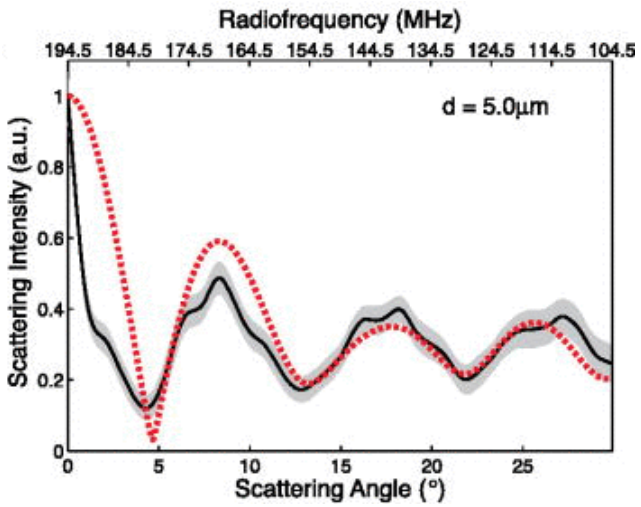
Radiofrequency (MHz)
194.5 184.5 174.5 164.5 154.5 144.5 134.5 124.5 114.5 104.5
d = 5.0µm
Scattering Intensity (a.u.)
Scattering Angle (°)

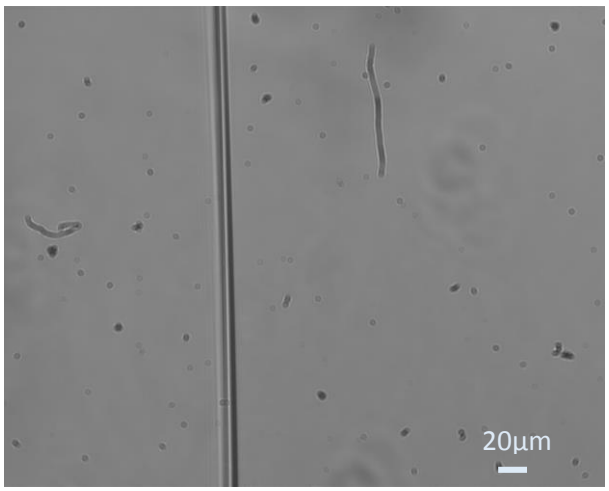
20µm

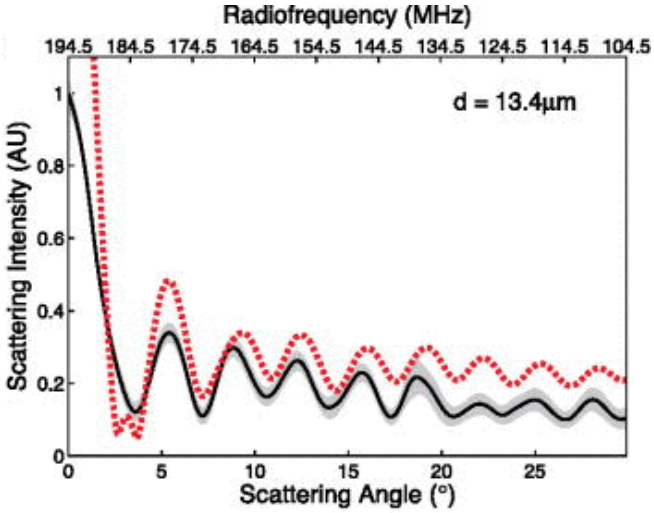
Radiofrequency (MHz)
194.5 184.5 174.5 164.5 154.5 144.5 134.5 124.5 114.5 104.5
d = 13.4µm
Scattering Intensity (AU)
Scattering Angle (°)

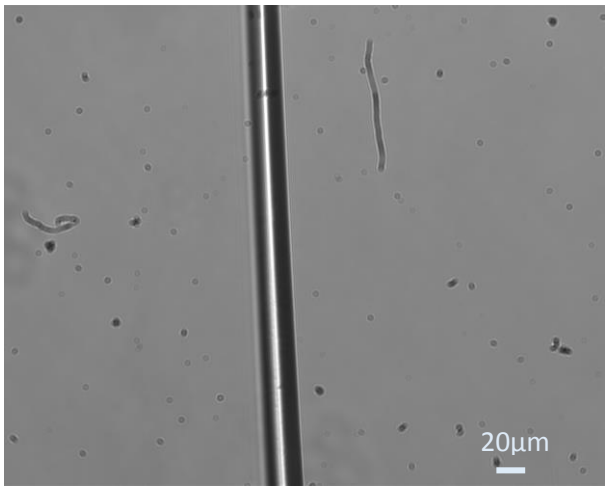
20µm

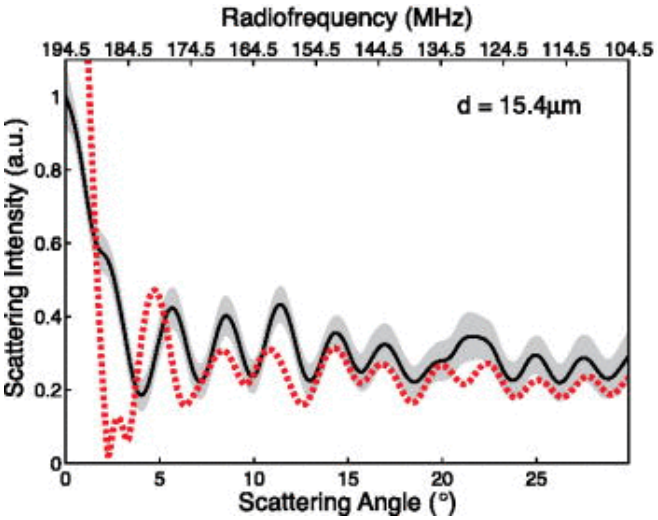
Radiofrequency (MHz)
194.5 184.5 174.5 164.5 154.5 144.5 134.5 124.5 114.5 104.5
d = 15.4µm
Scattering Intensity (a.u.)
Scattering Angle (°)

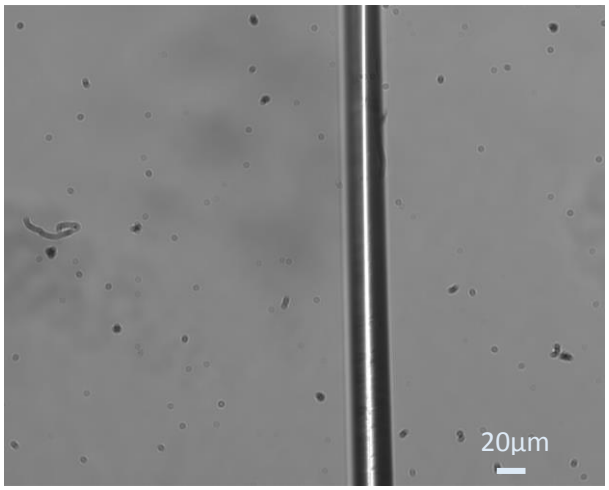
20µm

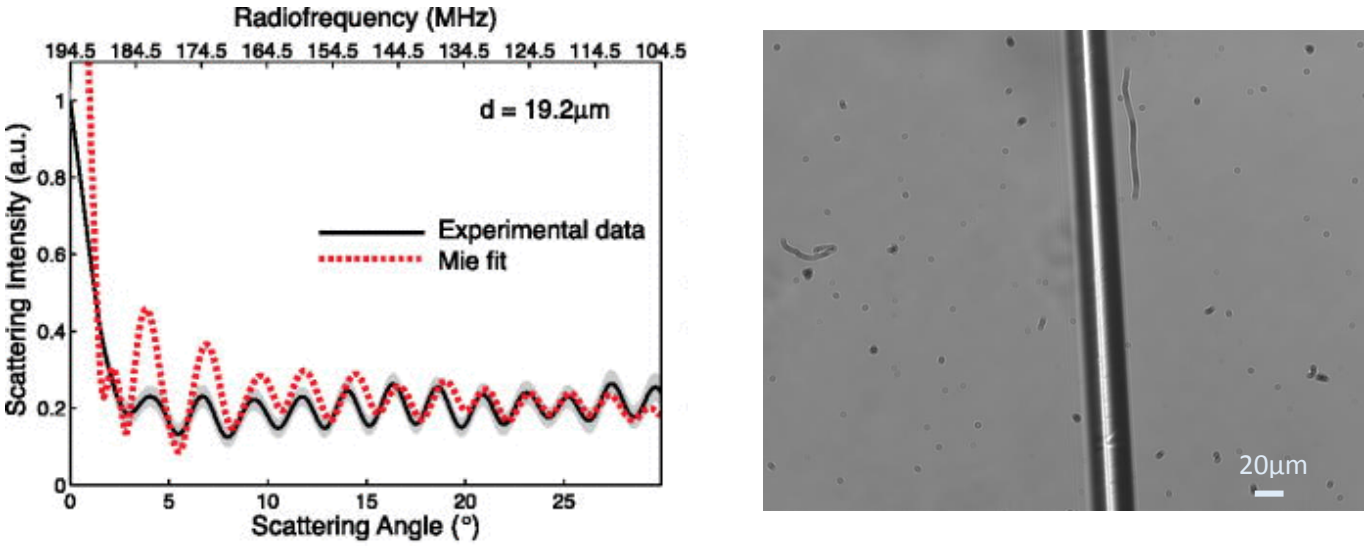

Figure 9 Scattering from a tapered silica optical fiber in air. These scattering profiles show the angular scattering spectrum from different locations on the taper, each measured at a rate of 250,000 spectra per second. These plots represent the mean (dark solid line) and standard deviation (gray shaded area) of 200 individual spectra. Each spectrum is taken using 91 discrete radiofrequencies. Mie scattering profiles were simulated and cylindrical diameters determined to best fit the measured scattering data. The diameters found with simulations match closely those of the tapered fiber sample, validating the ability of REALS to discern morphological structure from the scattering profile at high-speed and with high-resolution.

Conclusion

The presented proof-of-principle scattering measurements demonstrate the ability of REALS to resolve small changes in diameter for dielectric scattering objects. The width of the lobes in the scattering spectra increase with decreasing diameter as predicted by Mie theory. The variation in periodicity is a measure of object size. The data was acquired at a rate of 250 kHz. This acquisition speed corresponds to an event recording speed that is well above the capability of modern flow cytometers, making REALS an ideal addition to state-of-the-art systems. REALS has the capability to enable rapid, label-free scattering-based classification of cells, which could prove useful for many applications including stem cell research[22], clinical diagnostics[5,23–25], and high-resolution analysis of cellular sub-populations[26,27]. The current REALS implementation

demonstrates 1.1º scattering angle resolution (to 3.4 MHz RF frequency) detection resolution over 91-MHz RF bandwidth (~26 resolvable scattering angles) corresponding to 30º scattering angle range. The dynamic range of scattering angle detection can be significantly improved by using higher-resolution AODs[28], smaller detection pinhole system, and higher NA objective lenses enabling applications that require higher angular resolution or dynamic range.

References

1. Kutzsche, S., Ilves, P., Kirkeby, O. J. & Saugstad, O. D. Hydrogen Peroxide Production in Leukocytes during Cerebral Hypoxia and Reoxygenation with 100% or 21% Oxygen in Newborn Piglets. *Pediatr. Res.* **49,** 834–842 (2001).
2. Pan, Y.-L. *et al.* Measurement and autocorrelation analysis of two-dimensional light-scattering patterns from living cells for label-free classification. *Cytometry A* **79A,** 284–292 (2011).
3. Brunsting, A. & Mullaney, P. F. Light scattering from coated spheres: model for biological cells. *Appl. Opt.* **11,** 675–680 (1972).
4. Kerker, M. *et al.* Light scattering and fluorescence by small particles having internal structure. *J. Histochem. Cytochem.* **27,** 250–263 (1979).
5. Mourant, J. R. *et al.* Mechanisms of Light Scattering from Biological Cells Relevant to Noninvasive Optical-Tissue Diagnostics. *Appl. Opt.* **37,** 3586 (1998).
6. Meyer, R. A. Light scattering from biological cells: dependence of backscatter radiation on membrane thickness and refractive index. *Appl. Opt.* **18,** 585–588 (1979).
7. Marx, E. & Mulholland, G. W. Size and Refractive Index Determination of Single Polystyrene Spheres.
8. Soini, J. T., Chernyshev, A. V., Hänninen, P. E., Soini, E. & Maltsev, V. P. A new design of the flow cuvette and optical set-up for the scanning flow cytometer. *Cytometry* **31,** 78–84 (1998).

9. Chernyshev, A. V., Prots, V. I., Doroshkin, A. A. & Maltsev, V. P. Measurement of scattering properties of individual particles with a scanning flow cytometer. *Appl. Opt.* **34,** 6301 (1995).
10. Singh, K., Capjack, C., Rozmus, W. & Backhouse, C. J. Reply: Analysis of cellular structure by light scattering measurements in a new cytometer design based on a liquid-core waveguide. *IEE Proc. - Nanobiotechnology* **153,** 135 (2006).
11. Adam, J., Mahjoubfar, A., Diebold, E. D., Buckley, B. W. & Jalali, B. Spectrally encoded angular light scattering. *Opt. Express* **21,** 28960 (2013).
12. Goda, K., Tsia, K. K. & Jalali, B. Serial time-encoded amplified imaging for real-time observation of fast dynamic phenomena. *Nature* **458,** 1145–1149 (2009).
13. Goda, K. & Jalali, B. Dispersive Fourier transformation for fast continuous single-shot measurements. *Nat. Photonics* **7,** 102–112 (2013).
14. Konokhova, A. I., Gelash, A. A., Yurkin, M. A., Chernyshev, A. V. & Maltsev, V. P. High-precision characterization of individual *E. coli* cell morphology by scanning flow cytometry. *Cytometry A* **83A,** 568–575 (2013).
15. Konokhova, A. I. *et al.* Enhanced characterisation of milk fat globules by their size, shape and refractive index with scanning flow cytometry. *Int. Dairy J.* **39,** 316–323 (2014).
16. Bohren, C. F. & Huffman, D. R. *Absorption and scattering of light by small particles*. (Wiley, 1983).
17. Goodman, J. W. *Introduction to Fourier optics*. (Roberts & Co, 2005).
18. Liu, J.-M. *Photonic devices*. (Cambridge, 2005). at <http://www.books24x7.com/marc.asp?bookid=10818>

19. Diebold, E. D., Buckley, B. W., Gossett, D. R. & Jalali, B. Digitally synthesized beat frequency multiplexing for sub-millisecond fluorescence microscopy. *Nat. Photonics* **7,** 806–810 (2013).
20. Xiaojing Huang. Simple implementations of mutually orthogonal complementary sets of sequences. in 369–372 (IEEE, 2005). doi:10.1109/ISPACS.2005.1595423
21. Gattass, R. R., Svacha, G. T., Tong, L. & Mazur, E. Supercontinuum generation in submicrometer diameter silica fibers. *Opt. Express* **14,** 9408 (2006).
22. Sutherland, D. R., Anderson, L., Keeney, M., Nayar, R. & Chin-Yee, I. The ISHAGE Guidelines for CD34+ Cell Determination by Flow Cytometry. *J. Hematother.* **5,** 213–226 (1996).
23. Backman, V. *et al.* Detection of preinvasive cancer cells. *Nature* **406,** 35–36 (2000).
24. Liu, C., Capjack, C. & Rozmus, W. 3-D simulation of light scattering from biological cells and cell differentiation. *J. Biomed. Opt.* **10,** 014007 (2005).
25. Sem'yanov, K. A., Tarasov, P. A., Soini, J. T., Petrov, A. K. & Maltsev, V. P. Calibration-Free Method to Determine the Size and Hemoglobin Concentration of Individual Red Blood Cells from Light Scattering. *Appl. Opt.* **39,** 5884 (2000).
26. Zink, D., Fische, A. H. & Nickerson, J. A. Nuclear structure in cancer cells. *Nat. Rev. Cancer* **4,** 677–687 (2004).
27. Su, X.-T., Capjack, C., Rozmus, W. & Backhouse, C. 2D light scattering patterns of mitochondria in single cells. *Opt. Express* **15,** 10562 (2007).
28. Eddie H. Young, J. & Shi-Kay Yao. Design considerations for acousto-optic devices. *Proc. IEEE* **69,** 54–64 (1981).